Available online at www.sciencedirect.com
SCIENCE DIRECT®
International Journal of Thermal Sciences 42 (2003) 223–237
International Journal of Thermal Sciences
www.elsevier.com/locate/ijts

Investigation of the prechamber geometrical configuration of a natural gas spark ignition engine for cogeneration: part I. Numerical simulation

R.P. Roethlisberger, D. Favrat *

Laboratory for Industrial Energy Systems, Swiss Federal Institute of Technology of Lausanne, CH-1015 Lausanne, Switzerland

Received 7 September 2001; accepted 19 April 2002

Abstract

The effects and consequences of transferring the ignition point of the conventional combustion chamber into a small unscavenged prechamber were evaluated through a numerical simulation based on the CFD-code *KIVA-3V*. The prechamber flow characteristics at the location of the gap between the spark plug electrodes and in the crank angle period where the ignition is expected to occur were compared to the corresponding conditions in the conventional combustion chamber. The influence of the prechamber geometrical configuration was evaluated through variations of the nozzle orifice diameter, number and orientation, as well as prechamber volume and internal shape. The results show that the velocity magnitude is mainly dependent on the prechamber shape, and that it is generally of the same order as with direct ignition. Further, the turbulence intensity varies strongly with the geometrical configuration and reaches, in most cases, a much higher value in the prechamber. The partial dilution of the unburnt mixture with unscavenged prechamber residual gas generally leads to a slightly lower fuel to air equivalence ratio. However, nozzle orifices imparting a swirl motion or a prechamber shape with an almost uniform cross section can result in fuel concentration very close to or beyond the flammability limit. The prechamber charge and thereby the amount of energy available for the main chamber ignition depends on the prechamber volume and on the pressure drop across the nozzle orifices.

Keywords: Gas engine; Spark ignition; Unscavenged prechamber; Natural gas; Cogeneration; Numerical simulation; KIVA-3V

1. Introduction

When considering the decentralised power and heat generation (cogeneration), numerous applications have shown that small size spark ignition internal combustion engines operating on natural gas or biogas are able to achieve simultaneously an efficient and clean conversion of the primary energy. Among gaseous fuels, the high hydrogen to carbon ratio of natural gas results in a decrease of the CO_2 emissions generated per unit of final energy produced and biogas is CO_2 neutral. In consequence, cogeneration with gas engines is a particularly efficient way to save energy and to preserve the global environment. However, the more and more stringent legislation for exhaust gas emissions requires further improvement of the combustion process, particularly when catalytic after treatment is not reliable or considered too expensive.

With a limit of 250 $mg{\cdot}m_N^{-3}$, 5% O_2 (400 in the case of biogas operation) for NO_X and 650 $mg{\cdot}m_N^{-3}$, 5% O_2 for CO [1], Switzerland has the most stringent exhaust gas emissions regulation for stationary combustion engines in Europe. Several engine operating modes are able to fulfil these requirements, but the two mainly used in practice rely on catalytic exhaust gas after treatment. The first one is based on the use of a stoichiometric mixture and a three way catalyst. The second one corresponds to the lean burn mode with oxidation catalyst. These two modes were investigated in an earlier study [2,3]. The use of exhaust gas catalytic after treatment adds extra costs and increases the complexity of cogeneration systems, which tends to increase their maintenance costs and to lessen their reliability. In the case of engines operating only or partly on unprocessed sewage or landfill biogas, catalytic exhaust gas after treatment cannot be reliably used. Sewage and landfill gases contain significant amounts of sulfur and heavy metals, which rapidly deactivate the catalyst. Consequently, in order to achieve high reliability and to enable alternate operation on natural gas and biogas, it is

* Corresponding author.
E-mail address: daniel.favrat@epfl.ch (D. Favrat).
URL address: http://leniwww.epfl.ch.

1290-0729/02/$ – see front matter
doi:10.1016/S1290-0729(02)00023-6

Nomenclature

Symbols

A_n	total nozzle orifice area	mm^2
d_n	nozzle orifice diameter	mm
c	mass fraction	
k	turbulence kinetic energy	$m^2 \cdot s^{-2}$
N_n	number of nozzle orifices	
n	crankshaft rotational speed	rpm
p	pressure	bar
S	mean piston speed	$m \cdot s^{-1}$
T	temperature	K
V_c	compression volume	mm^3
V_p	prechamber volume	mm^3
v	flow velocity	$m \cdot s^{-1}$

Greek symbols

α_n	nozzle orifice mean angle	°
Δp	pressure difference	bar
ϕ	fuel to air equivalence ratio	

Subscripts

ABDC	after bottom dead centre
ATDC	after top dead centre
BBDC	before bottom dead centre
BTDC	before top dead centre

Abbreviations

CA	crank angle
p	piston
TDC	top dead centre

necessary to decrease the exhaust emissions below the Swiss limits for natural gas operation at the level of the combustion process.

This motivated the investigation of the use of an unscavenged prechamber for application on a small size cogeneration gas engine in order to evaluate the potential to reduce simultaneously the NO_X and CO emissions, while maintaining the fuel conversion efficiency at a high level. The objective of this article is to present the results of a numerical simulation of the influence of the prechamber geometrical configuration on the flow conditions at the location of the spark plug electrodes during the compression stroke (no combustion simulation). This was realised with the CFD-code *KIVA-3V* through variations of the number, size and orientation of the prechamber nozzle orifices as well as of the prechamber internal volume and shape. The purpose of the numerical study was to assist the selection of the most promising configurations for experimentation. More precisely, the simulation was intended to avoid testing configurations, which could lead to excessive flow velocity or turbulence intensity or to too low fuel concentration at the location of the spark plug electrodes and thus to result in nonpracticable ignition conditions. The selection was operated on the basis of the experimental results of a first configuration and the trend shown by the simulation. The objective of the simulation was further to help the interpretation of the experimental results. Because the combustion and the pollutant formation were not modelled, the simulation could not directly be used to determine an optimal theoretical prechamber geometrical configuration. The experimental results are published in part II [4].

2. Engine specifications and prechamber design

The engine used is derived from a *Liebherr* heavy duty diesel engine type 926 converted for natural gas operation on the *Otto* principle and is intended for cogeneration applications. The main engine specifications are summarised in Table 1. The engine is equipped with new cylinder heads, which enable the fitting of spark plugs at the location of the diesel injectors. The combustion chamber was adapted to the spark ignition operation through a modification of the piston bowl shape and a decrease of the volumetric compression ratio from 17.2 to 12.0 (Fig. 1(a)). The engine is turbocharged and intercooled.

Table 1
Main engine specifications

Manufacturer	Liebherr	Number of valves	2
Type	G 926 TI	Intake valve opening	15° CA_{BTDC}
Number of cyl.	6 in line	Intake valve closing	45° CA_{ABDC}
Bore	122 mm	Exhaust valve opening	54° CA_{BBDC}
Stroke	142 mm	Exhaust valve closing	14° CA_{ATDC}
Conrod length	228 mm	Swirl ratio [5, Eq. (8.28)]	2.0
Total swept vol.	9.96 l	Vol. compression ratio	12.0

A small water cooled prechamber, representing 2 to 3% of the main chamber compression volume, was designed to be housed in the boss of the existing cylinder head used for the spark plug well. The prechamber integrated to the modified cylinder head is represented in Fig. 1(a). More detailed information on the engine conversion and on the prechamber design and cylinder head modifications can be found in [6].

3. Simulation procedure

The simulation procedure is based on the use of the CFD-code *KIVA-3V* [7]. The mesh generation was realised with the software *HEXA* by *ICEMCFD* and the results visualisation was done with the program *EnSight 6* by *CEI*. The use of these two softwares required the implementation of different interfaces to link them to the CFD-code

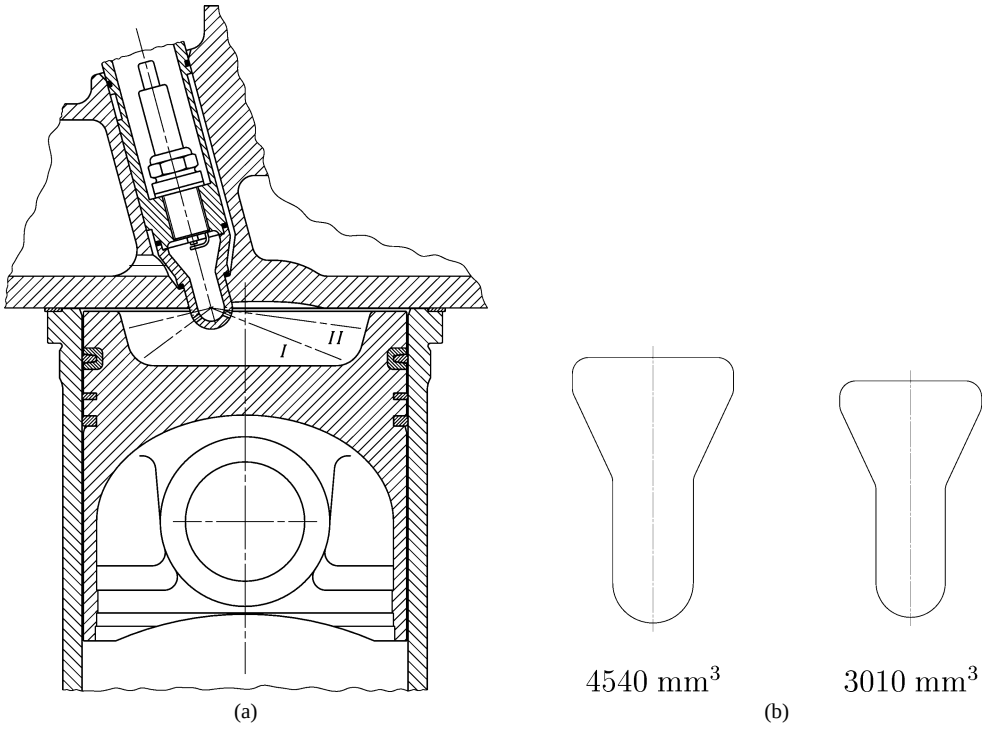

Fig. 1. (a) schematic representation of the combustion chamber with prechamber ignition and original piston for natural gas operation, indicating the two nozzle orientation experimentally investigated, (b) two different volumes of the prechamber internal geometries studied.

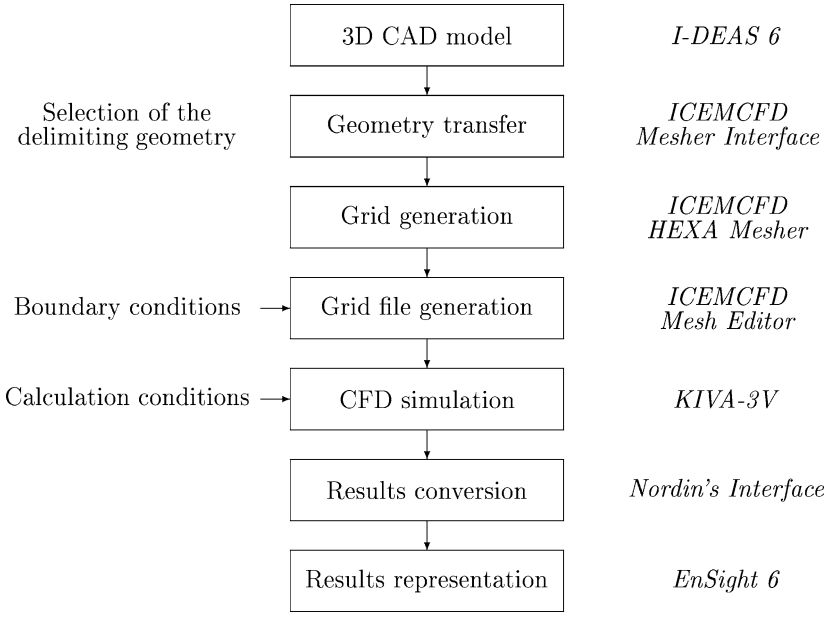

Fig. 2. CFD simulation procedure.

and to link the mesh generator to the 3D-CAD program *I-DEAS 6* by *SDRC* for the geometry transfer. The visualisation of the simulation results required a preliminary conversion of the *KIVA-3V* output file to a suitable format for *EnSight 6*. This was realised with the help of an interface written by Nordin [8], freely available on the World Wide Web. The complete simulation procedure is summarised in Fig. 2.

KIVA-3V was used as a development tool and the source code was not modified. A detailed description of the sofware is beyond the scope of this study but can be found in the code manuals [7,9,10].

For constructive reasons, the designed combustion prechamber is tilted and its nose is set off the main combustion chamber axis, thus forming a nonaxisymetrical configuration (Fig. 1(a)). A numerical simulation based on the real

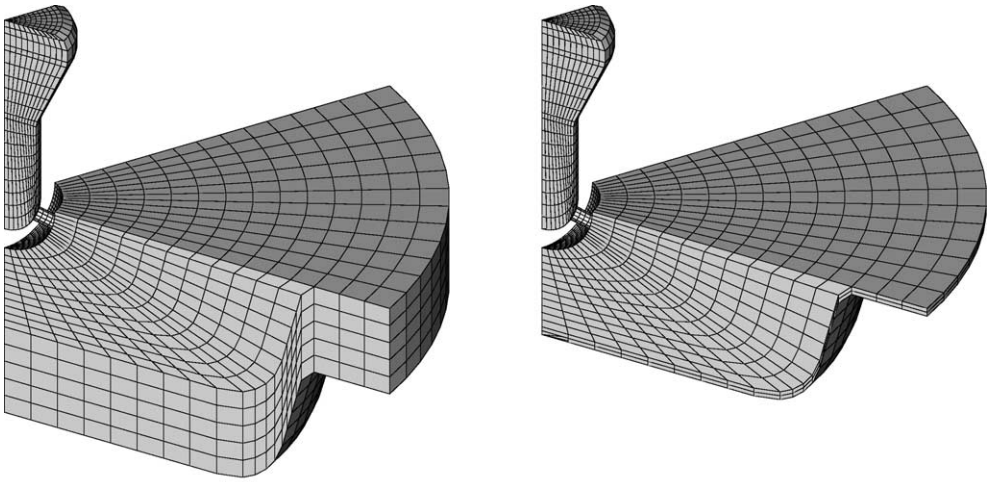

Fig. 3. Mesh of the computational domain: (a) at 30° CA_{BTDC}, (b) at TDC.

geometry would lead to a prohibitive computation time, mainly because of numerous small cells required for an adequate mesh resolution in the prechamber and in the nozzle orifices. The way to overcome the actual computer limits is to consider an axisymetrical geometry and to simulate only a periodic sector including a single nozzle orifice. The principal drawback of this simplification is to neglect the influence of the asymmetry on the prechamber flow pattern. The change in numerical solution resulting from variations of the nozzle parameters should give some indication on the influence of the asymmetry.

The mesh generation is performed on the geometry of the combustion chamber when the piston is positioned at bottom dead centre. This operation requires the fulfilment of certain *KIVA* specific rules for the part of the mesh located in the squish region and undergoing an adjustment procedure (snapping) during the simulation. These rules specify that all the grid lines in the squish region must be vertical in the z-direction [10, p. 94] and horizontal in the y-direction, around the periphery of the cylinder [9, p. 32]. On the other hand, the radial grid lines do not need to be horizontal (x-direction). To satisfy these rules, the fixed cells commonly located in the piston bowl in conventional combustion chamber mesh have to be attached to the cylinder head, around the prechamber nose. According to the *KIVA* denomination, these cells as well as the one located in the prechamber and in the nozzle orifice must be defined as belonging to the dome in cylinder head.

The main objective of the numerical simulation was to study the flow in the prechamber during the compression stroke. This required a particular refinement of the corresponding part of the mesh to achieve an adequate resolution. On the other hand, the mesh in the main combustion chamber was kept relatively coarse to reduce the computing time. The final mesh resolution was chosen on the basis of a sensitivity analysis, which showed that the mesh heterogeneity has no adverse consequence on the numerical solution in the prechamber because of the strong filtering effect of the small nozzle orifice. A typical mesh for a 60° sector is given in Fig. 3 at two different crank angles. The total number of cells is 8 714, with 1 499 cells in the prechamber (including the nozzle orifice) and 7 215 cells in the main chamber. The meshs for other angles of sector (change of the number of nozzle orifices) were realised through a proportional adjustment of the number of azimuthal cells. Two distinct fluid regions have been defined in order to enable different initial conditions in the main- and prechamber.

Table 2
Main calculation and initial conditions

	Main chamber		Prechamber
Region	1		2
n		1500 rpm	
$T_{\text{cyl. wall}}$	180 °C		–
$T_{\text{cyl. head}}$	180 °C		180 °C
T_{piston}	280 °C		–
p		2.63 bar	
T	105 °C		205 °C
k		12.6 $m^2 \cdot s^{-2}$	
ϕ	0.565		0.000
c_{CH_4}	0.028		0.0000
c_{O_2}	0.2123		0.0979
c_{N_2}	0.7431		0.7431
c_{CO_2}	0.0087		0.0874
c_{H_2O}	0.0072		0.0716

The calculation and initial conditions have been kept constant during the geometrical parametric study and the main values are summarised in Table 2. The purpose of the numerical simulation was to study the influence of geometrical parameters on the flow field inside the prechamber during the compression stroke and particularly in the ignition window (crank angle domain where ignition is expected to occur). Therefore, the simulation was limited to a non-reacting mixture of fuel, air and residual gas from the

previous cycle. To reduce the number of species involved, the practical fuel, natural gas, was substituted by methane, its main component. The simulated angular domain extends from 130° CA_{BTDC} (5° CA after inlet valve closure) to 30° CA_{ATDC}. At the beginning of the simulation, the main combustion chamber was filled with an unburnt mixture of methane and air, containing 10% residual gas of a complete combustion. The prechamber was filled exclusively with residual gas. The fuel to air equivalence ratio and the initial pressure and temperature were derived from experimental results of the engine equipped with the conventional combustion chamber (same piston, direct ignition), operating at a power output of 150 kW, a crankshaft rotational speed of 1500 rpm and minimum NO_X emissions. The pressure distribution at the beginning of the simulation (shortly after inlet valve closure) was considered uniform throughout the whole combustion chamber. The prechamber temperature was assumed 100 °C above the calculated main chamber value.

Because the flow through the inlet port during the intake stroke does not generate a significant swirl motion in the prechamber and *KIVA-3V* does not allow the definition of different swirl conditions in the distinct fluid regions, the simulation was performed without initial swirl motion. The cylinder wall, cylinder head and piston temperatures were derived from experimental results in conventional lean burn operating mode. The renormalised group (RNG) theory k–ε model was selected to simulate the flow turbulence and the initial turbulence kinetic energy was chosen equal to 50% of the value based on the mean piston speed ($k_{S_p} = 0.5S_p^2$). *KIVA-3V* has been implemented on a *Silicon Graphics* (*SGI*) *Origin 2000*, equipped with 195 MHz *MIPS R10000* processors. The computation was performed sequentially on a single processor and the resolution rate was about 55 MFlops, leading to a total execution time of mainly less than 30 CPU hours, but sometimes up to 80 CPU hours. This large execution time is due to the time step restriction (1 to 2×10^{-7} s) imposed by the presence of some very small cells in the prechamber mesh.

4. Results and discussion

This section shows the effect on the flow conditions at the location of the spark plug electrodes of transferring the ignition point into a prechamber. Further, it presents and discusses the influence of the number, size and orientation of the prechamber nozzle orifices as well as of the prechamber internal volume and shape on the prechamber flow conditions during the compression stroke, and particularly on the ignition conditions. Three particular positions in the plane of symmetry going through the centre of the nozzle orifice were selected (Fig. 4) for the interpretation of the results. The first location (I) corresponds to the position between the spark plug electrodes (spark plug electrodes not modelled) and gives an indication of the conditions

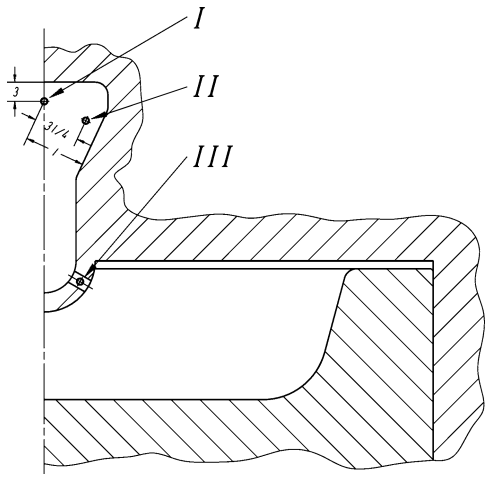

Fig. 4. Reference locations in the combustion prechamber.

that prevail during the ignition process and the early stage of the flame kernel growth. The second position (II) is located close to the middle of the main prechamber recirculation zone and is consequently a sensitive indicator of changes in the main flow pattern. The third point (III) is located in the middle of the nozzle orifice and gives information on the flow conditions at this particular position.

4.1. Comparison between direct and prechamber ignition conditions

In order to evaluate the effect of transferring the ignition location into a prechamber, the flow in the conventional combustion chamber equipped with the original piston (*A*) (Fig. 1(a)) and alternatively with a high turbulence generating piston with re-entrant bowl (*B*) was simulated and compared to the numerical results of the first prechamber design. The simulation was based on 60° sector mesh comprising 8164 and 8736 cells in the case of piston *A* and *B*, respectively. The initial calculation conditions were identical to the prechamber case (Table 2), except for the swirl ratio which was fixed at 2.0 (Table 1). The flow characteristics at the location between the spark plug electrodes are represented for the different cases in Fig. 5. The actual optimal spark timing for minimum NO_X emissions in the conventional combustion chamber is 26.7° CA_{BTDC}.

The flow velocity at the prechamber spark location increases during the compression stroke to reach its maximum value in the ignition window (Fig. 5(a)). However, the velocity remains lower than in the conventional combustion chamber at the optimal spark timing, independently of the piston used. The lower flow velocity prevents an excessive stretching of spark and of the initial flame kernel, thus reducing the probability of ignition failure. The high turbulence generated by the nozzle jets and diffusing in the prechamber reaches an intensity up to twice the value characterising the conventional combustion chamber at optimal spark timing (Fig. 5(b)). Higher turbulence intensity pro-

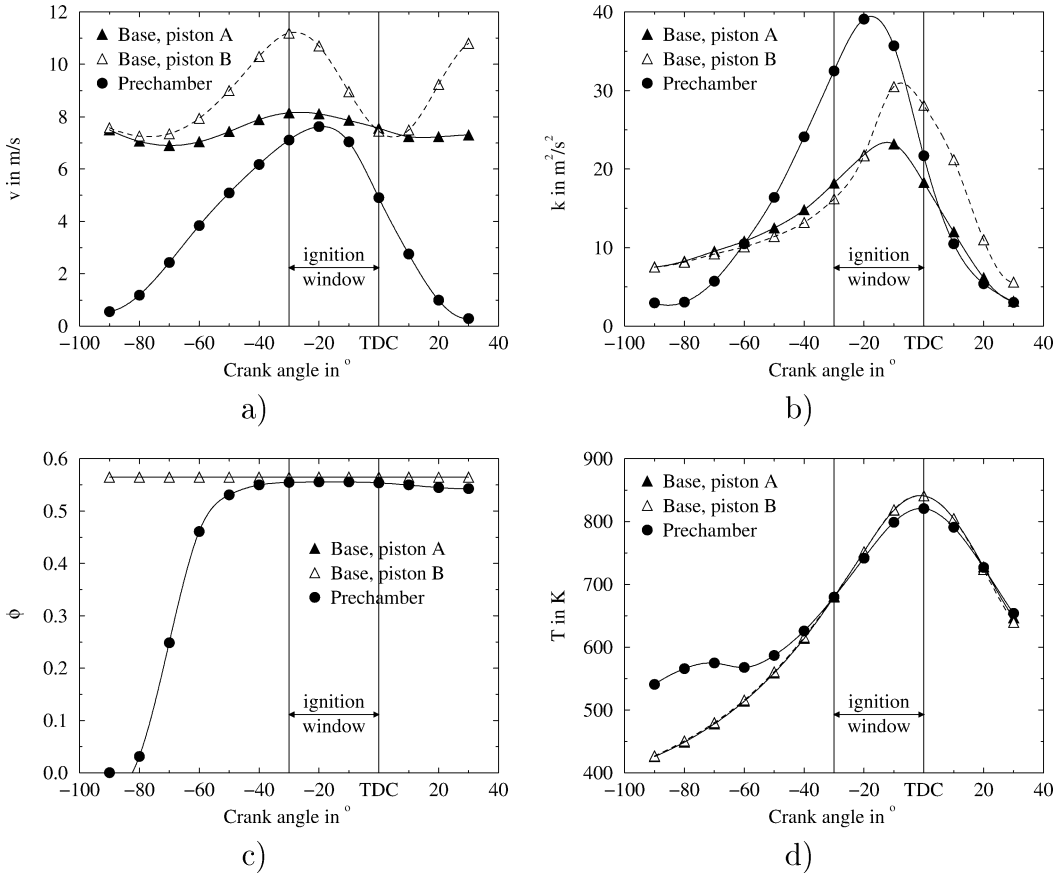

Fig. 5. Comparison of the flow conditions at the location of the spark plug gap between conventional combustion chamber (base, pistons A and B) and prechamber ($V_p = 4540$ mm^3, $d_n = 2$ mm, $N_{n=6}$, $A_n = 18.85$ mm^2, $\alpha_n = 60°$): (a) velocity magnitude, (b) turbulence kinetic energy, (c) fuel to air equivalence ratio, (d) temperature.

motes the combustion process but also perturbs the ignition arc discharge phase and the initial flame kernel generation [11]. Through the progressive replacement of the residual gas by the fresh incoming mixture, the fuel to air equivalence ratio increases rapidly to reach an almost constant value in the ignition window (Fig. 5(c)). Because of complementary dilution with residual gas, the maximum value is slightly lower than in the case of the conventional combustion chamber. The prechamber temperature remains at first relatively constant because of the mixing with cooler fresh incoming mixture and then increases due to compression (Fig. 5(d)). In comparison to the conventional combustion chamber, it reaches a somewhat lower maximum value at TDC. The difference in peak temperature originates in the stronger heat transfer to the prechamber resulting from the larger surface to volume ratio and the higher turbulence intensity. Depending on the complementary spark timing delay allowed by the use of a prechamber, the temperature at the time of ignition will be similar or higher than the one in the conventional combustion chamber. A higher temperature will promote ignition and accelerate the initial flame kernel growth.

4.2. Nozzle orifice cross-sectional area

The total nozzle orifice cross-sectional area of the base prechamber design (18.85 mm^2) was decreased and then increased by 50%, alternatively. The orifice diameter was consequently reduced to 1.41 mm ($A_n = 9.42$ mm^2) and increased to 2.45 mm ($A_n = 28.27$ mm^2), respectively. The mesh was adjusted to accommodate the variation of orifice diameter, without change in the number of cells.

The increase of total cross-sectional area yields a strong reduction of nozzle flow velocity (Fig. 6(a)) and consequently leads to a drastic decrease of turbulence generation (Fig. 6(b)). This causes a significant reduction of turbulence intensity in the upper prechamber part (I and II). The increase of total cross-sectional area strongly reduces the pressure drop between main- and prechamber (Fig. 6(d)). This yields an increase of incoming mass flow, which results in a somewhat higher velocity at the ignition location (I). The relative stability of the velocity in the main recirculation zone (II) indicates no significant variation of the main flow pattern. The increase of axial velocity accelerates the transfer of unburnt mixture at the prechamber top, but has no noticeable effect on the fuel to air equivalence ratio in the ignition window (Fig. 6(c)). Finally, due to the reduction of

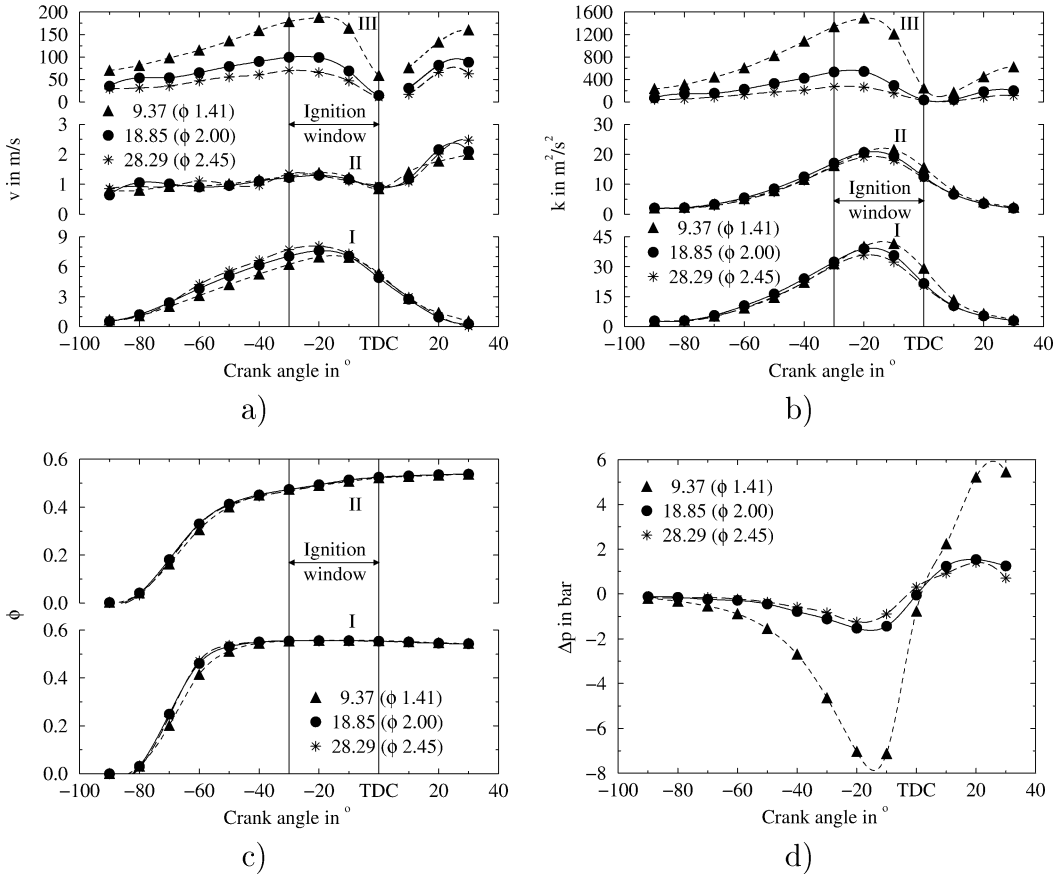

Fig. 6. Influence of the total cross-sectional area of the nozzle orifices on the flow at different locations in the prechamber ($V_p = 4540$ mm^3, $N_n = 6$, $\alpha_n = 60°$): (a) velocity magnitude, (b) turbulence kinetic energy, (c) fuel to air equivalence ratio, (d) pressure difference between pre- and main chamber.

pressure drop, the increase of total cross-sectional area enables a more extensive prechamber filling. However, a larger amount of unburnt mixture will also be expelled again in the main chamber prior to completion of the prechamber combustion. Thus, the eventual benefit of larger orifices in this regard will essentially depend on the prechamber combustion characteristics.

4.3. Nozzle orifice orientation

In the base prechamber design, the orientation of each nozzle orifice from the prechamber axis (smallest angle between the orifice and prechamber axes, when both are in the same plane) was determined in order to point towards the bottom corner of the piston bowl, when the piston is located at TDC (Fig. 1(a), orientation I). The objective was to achieve a relatively uniform distribution of the jets of combustion products issuing from the prechamber into the clearance volume. The angle is different for each orifice and the average value is about 60°. This value was considered for the simulation of the base prechamber. Due to its significant influence on the main chamber combustion process and therefore on the engine performance and exhaust emissions [12,13], the nozzle orifice orientation was varied by ±15° from the base value of 60°. The mesh was adjusted consequently, while keeping the number of cells constant.

A larger orientation angle causes a greater local reorientation of the main chamber flow towards the nozzle orifices, which produces more turbulence (Fig. 7(b)). This does not affect the velocity magnitude in the nozzle orifices (III) (Fig. 7(a)), but significantly increases the pressure drop between main chamber and prechamber (Fig. 7(d)). On the one hand, the increase of the orientation angle increases the proportion of turbulence dissipated in the recirculation volume located at the prechamber bottom and consequently reduces the turbulence intensity in the upper part. This effect is more pronounced for the transition from 45° to 60° than further to 75°. On the other hand, it increases the size of the annular recirculation zone at the nozzle exits and thereby reduces the effective flow cross section in the prechamber lower part. This causes an increase in axial velocity that is partly compensated by the mass flow reduction associated with the increase in pressure drop. This finally results in a slight velocity increase at the ignition point (I), but does not significantly affect the main flow pattern (II) (Fig. 7(a)). A somewhat higher prechamber axial velocity compensates the reduction in mass flow and enables a similar transfer of unburnt mixture to the ignition region (Fig. 7(c)).

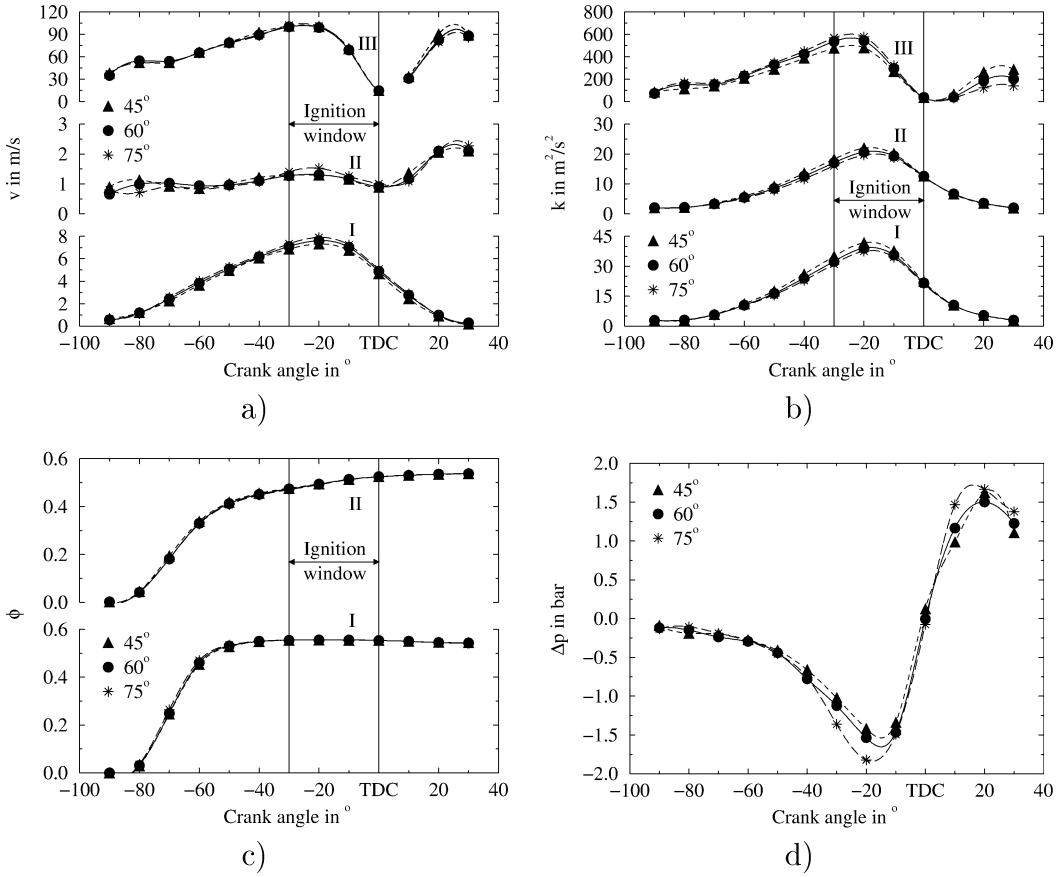

Fig. 7. Influence of the nozzle orifice orientation on the flow at different locations in the prechamber ($V_p = 4540$ mm^3, $d_n = 2$ mm, $N_n = 6$, $A_n = 18.85$ mm^2): (a) velocity magnitude, (b) turbulence kinetic energy, (c) fuel to air equivalence ratio, (d) pressure difference between pre- and main chamber.

4.4. Prechamber swirl

Imparting a swirling motion to the combustion chamber charge accelerates considerably the combustion process through an extension of the flame surface [5]. In the case of an engine with prechambers, part of the swirl motion can also be produced by the jet of combustion products emerging from suitably oriented nozzle orifices. During the compression stroke, this particular nozzle configuration also produces a swirl motion in the prechamber. In order to evaluate its effect on the flow characteristics, the nozzle orifices were rotated by an angle of 15° about an axis parallel to the prechamber one and passing through the orifice centre of gravity. The mesh was adjusted to the new configuration, while the number of cells was kept constant.

The flow characteristics in the nozzle orifices (III) are not significantly affected by their inclination (Fig. 8(a) and (b)). The inclination induces a strong swirling motion, which yields a fundamental change in the prechamber flow pattern (Fig. 8(a), locations I and II). Due to its position on the prechamber axis, the flow at the ignition point becomes almost stagnant when approaching TDC. The corresponding turbulence kinetic energy increases progressively towards the end of the compression stroke (Fig. 8(b)). However, the level reached in the major part of the ignition window is much lower than in the case of the base prechamber. The compression and stagnation of the residual gas at the prechamber top centre results in a much lower fuel to air equivalence ratio at the ignition point (Fig. 8(c)), which may be beyond the lean flammability limit. The generation of the swirl motion causes an increase in main flow kinetic energy which is compensated by a decrease of prechamber pressure (energy conservation). This is illustrated by the increase of the pressure drop between main- and prechamber (Fig. 8(d)).

4.5. Number of nozzle orifices

Starting from the base prechamber design, the number of nozzle orifices was reduced from 6 to 4 and increased to 8, respectively. In order to maintain similar flow conditions between main- and prechamber, the total nozzle orifice cross-sectional area was kept constant (18.85 mm^2) through adaptation of the orifice diameter. This resulted in 4 orifices of ∅2.45 mm and in 8 orifices of ∅1.73 mm. The angle of the sector mesh was increased to 90° in the case of 4 orifices and reduced to 45° in the case of 8 orifices. The mesh resolution was kept approximately constant through a proportional adjustment of the number of azimuthal cells; 7 604 and 11 352 cells for 45° and 90°, respectively.

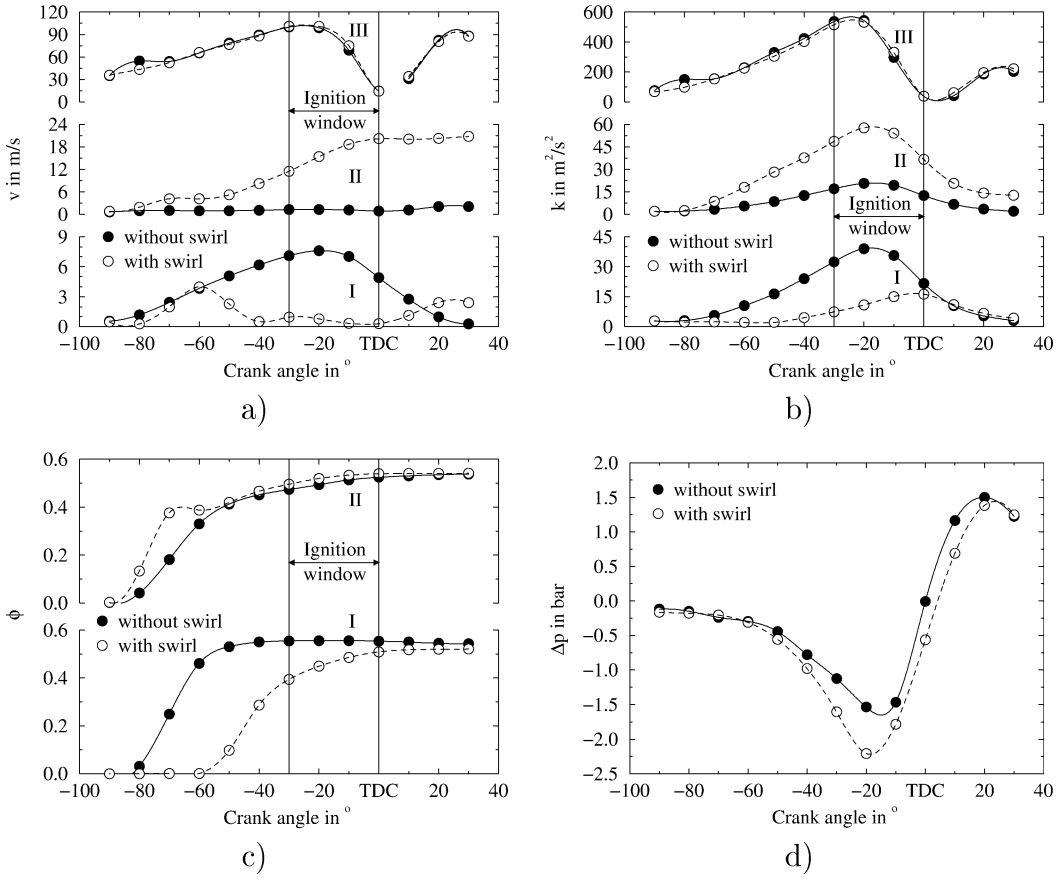

Fig. 8. Effect of a prechamber swirl motion generated by a 15° azimuthal inclination of the nozzle orifices on the flow at different locations in the prechamber ($V_p = 4540$ mm^3, $d_n = 2$ mm, $N_n = 6$, $A_n = 18.85$ mm^2, $\alpha_n = 60°$): (a) velocity magnitude, (b) turbulence kinetic energy, (c) fuel to air equivalence ratio, (d) pressure difference between pre- and main chamber.

An increase in the number of nozzle orifices multiplies the sources of turbulence generation. This results in a higher turbulence intensity in the upper prechamber part and particularly in the vicinity of the ignition point (I) (Fig. 9(b)). The effect is more pronounced in the case of a transition from 4 to 6 orifices than further to 8. The multiplication of the orifices yields an increase in axial velocity, which also affects the conditions at the ignition point (Fig. 9(a)). However, the weak velocity variation in the main recirculation zone (II) indicates no significant change in the flow pattern. Due to the higher axial velocity, the unburnt mixture reaches the prechamber top earlier (Fig. 9(c)). Nevertheless, this has no perceptible influence on the fuel to air equivalence ratio in the ignition window. The adjustment of the orifice diameter in order to keep the total cross-sectional area constant results in the same nozzle flow characteristics (III) and almost identical pressure drop between main- and prechamber (Fig. 9(d)).

4.6. Addition of a coaxial nozzle orifice

A more uniform distribution of the jets of combustion products issuing from the prechamber into the main chamber can be realised through the addition of a complementary nozzle orifice located coaxially at the prechamber bottom. In order to maintain the total nozzle orifice cross-sectional area constant and equal to the value of the base prechamber (18.85 mm^2), the orifice diameter was reduced from 2 to 1.85 mm. The mesh was modified to integrate the complementary orifice. The presence of the coaxial nozzle creates a direct connectivity between the main- and prechamber mesh blocks in such a way that their respective number of azimuthal cells can no longer be set independently. In order to keep the prechamber mesh resolution as close as possible to the base case, its azimuthal cells distribution was also applied to the main chamber. This resulted in a reduction of the total number of cells from 8 714 to 5 769.

In comparison to the base configuration, the presence of a coaxial orifice adds a new annular recirculation zone to the flow. However, this reduces strongly the size of the bottom recirculation volume and consequently the local dissipation of turbulence. The better coaxial orifice alignment to the main chamber flow results in a higher nozzle velocity compared to the tilted one (Fig. 10(a)). The overall lower turbulence generation is largely over-compensated by the reduction of dissipation in the prechamber bottom and leads to a much higher turbulence intensity in the upper prechamber part (Fig. 10(b)). On the other hand, the global

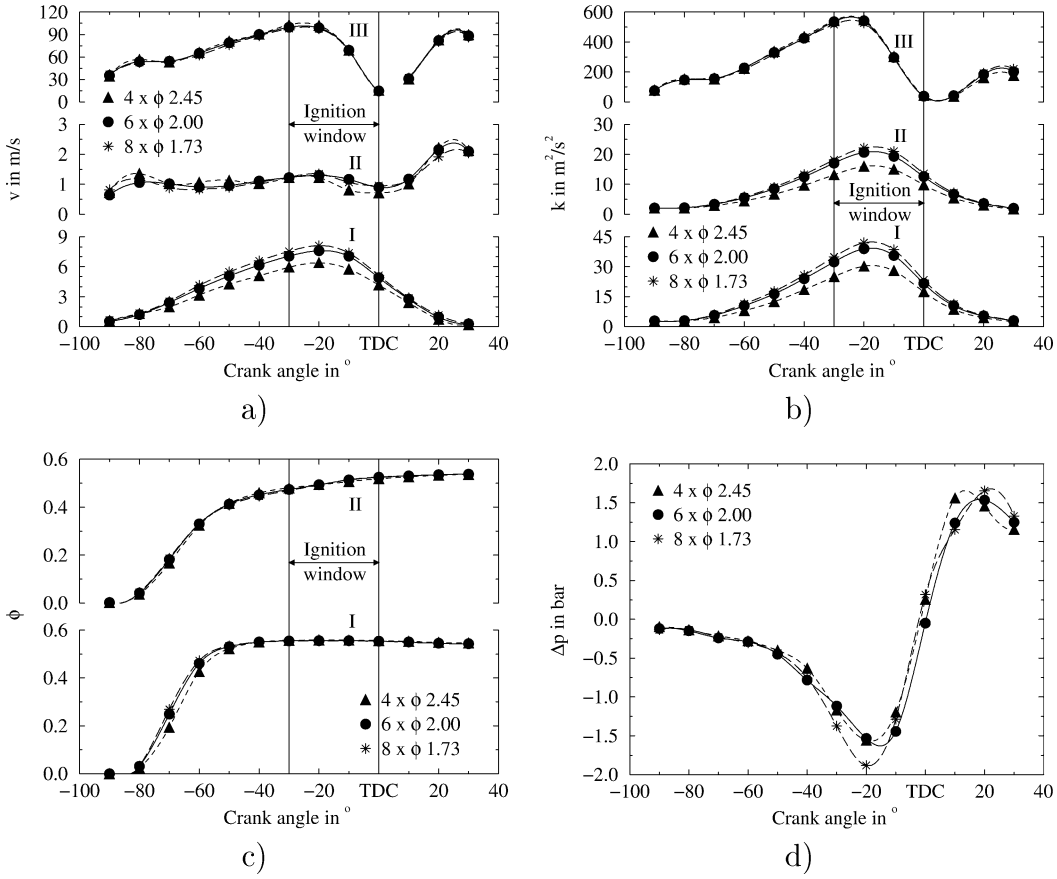

Fig. 9. Influence of the number of nozzle orifices at different locations in the prechamber ($V_p = 4540$ mm^3, $A_n = 18.85$ mm^2, $\alpha_n = 60°$): (a) velocity magnitude, (b) turbulence kinetic energy, (c) fuel to air equivalence ratio, (d) pressure difference between pre- and main chamber.

prechamber flow pattern and velocity magnitude in the upper prechamber part are only slightly affected. A somewhat higher axial velocity in the lower prechamber part accelerates the transfer of unburnt mixture towards the ignition region (Fig. 10(c)). The more intense local turbulence also enhances the incorporation of residual gas into the unburnt mixture, which results in a slightly lower maximum fuel to air equivalence ratio in the ignition window. The very similar global pressure drop between main- and prechamber during compression indicates an approximately similar prechamber filling (Fig. 10(d)).

4.7. Prechamber internal volume

The internal volume of the base prechamber (4540 mm^3) corresponds to 2.9 % of the total compression volume (clearance and prechamber volumes). Typical prechamber volumes used in heavy duty gas engine operating with stratified charge ranges from 1.5 to 5% of the clearance volume [12, 14–17]. In order to evaluate the influence of this parameter, the prechamber internal dimensions were proportionally reduced to obtain a volume of 3 010 mm^3, corresponding to 1.9% of the compression volume (Fig. 1(b)). Two different cases were studied. In the first case, the nozzle orifice diameter remained unchanged. In the second case, the ratio between the total nozzle orifice cross-sectional area and the prechamber internal volume (A_n/V_p) was kept constant, what theoretically leads to a constant pressure drop between pre- and main chamber [18]. In the later case, this leads to a reduction of the orifice diameter from 2.00 to 1.63 mm. The mesh was adjusted to the new geometry, while the total number of cells was not changed.

The proportional reduction of the prechamber dimensions in order to obtain a smaller internal volume results in a similar flow pattern and velocity magnitude in the upper prechamber part (Fig. 11(a)). In the case of the small prechamber, the reduction of the nozzle orifice diameter leads to a strong increase of the orifice flow velocity, which reaches values very close to the large prechamber one. In turn, this causes an important increase in turbulence generated. However, the level achieved remains significantly lower than in the case of the large prechamber (Fig. 11(b)). The decrease of the internal diameter of the lower prechamber part causes a significant increase in turbulence dissipation at the prechamber bottom. In the case of the large nozzle orifices, the decrease in the turbulence generated combined to the higher turbulence dissipation leads to a drastic reduction of the turbulence intensity in the upper prechamber part. Further, the higher turbulence generated through the reduction of the nozzle orifice diameter is largely dissipated in

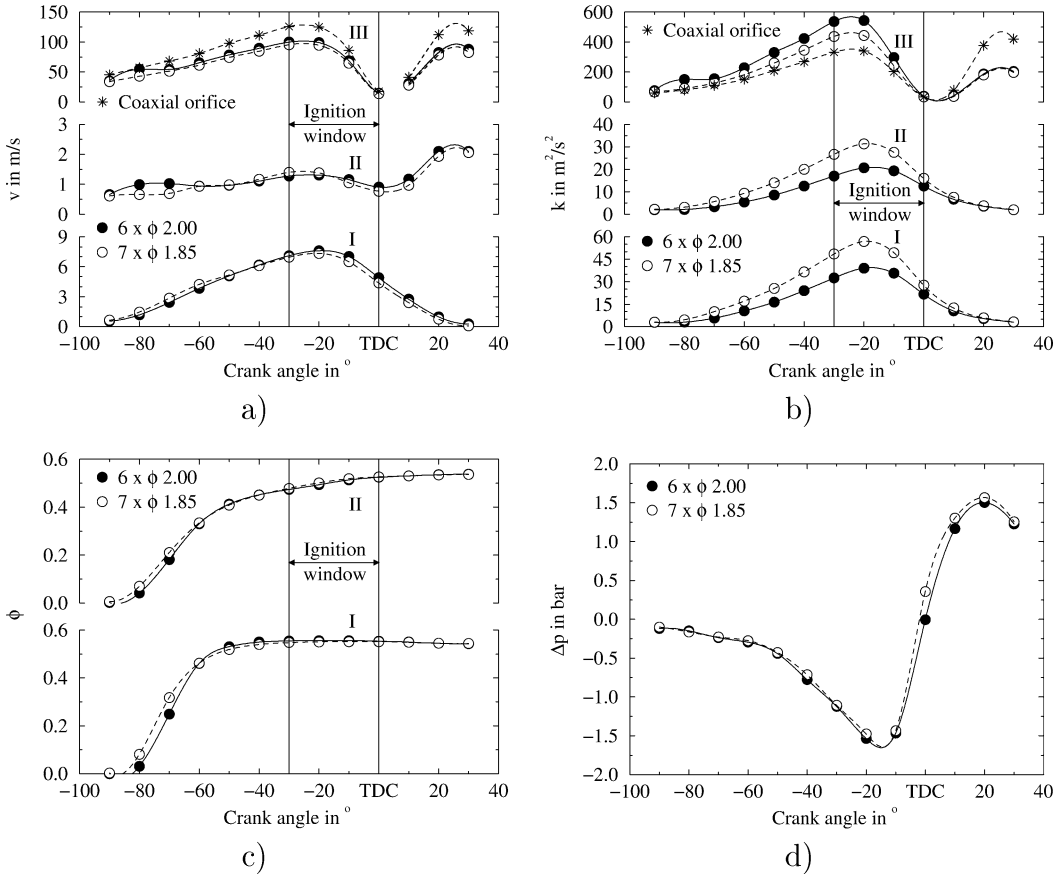

Fig. 10. Effect of a coaxial nozzle orifice on the flow at different locations in the prechamber ($V_p = 4540$ mm^3, $A_n = 18.85$ mm^2, $\alpha_n = 60°$): (a) velocity magnitude, (b) turbulence kinetic energy, (c) fuel to air equivalence ratio, (d) pressure difference between pre- and main chamber.

the lower prechamber part. However, it enables a further diffusion towards the prechamber top, which results in a somewhat higher turbulence intensity in the upper prechamber part. In the case of the reduced internal volume, the unburnt mixture reaches the prechamber top somewhat earlier, but without affecting the fuel to air equivalence ratio in the ignition window (Fig. 11(c)). In the case of a constant nozzle orifice diameter, the decrease of prechamber volume reduces significantly the pressure drop across the nozzle orifices (Fig. 11(d)). On the other hand, when the ratio A_n/V_p is kept constant, the pressure drop across the orifices remains the same up to 40° CA_{BTDC} and then increases significantly. Although a fixed ratio A_n/V_p does not enable the achievement of a similar pressure drop across the orifices during the whole compression phase, it enables to obtain reasonably similar nozzle orifice flow conditions. Therefore, keeping a constant ratio A_n/V_p is expected to better isolate the effect of the reduction of the internal volume.

4.8. Prechamber bottom geometry

During the compression stroke, the jets emerging into the base prechamber interact with the bottom geometry (geometry of the lowest part of the prechamber internal volume) to form annular recirculation zones. This type of flow induces losses which are detrimental to a rapid transfer of the fresh mixture to the ignition location and an efficient filling of the prechamber. In consequence, the base prechamber geometry (α) was modified in a first stage to suppress the bottom recirculation volume (Fig. 12, β) and in second stage to better lead the flow towards the prechamber top (γ). The mesh was adjusted to the geometry variations, without change in the number of cells.

A better leading of the incoming flow strongly increases the axial velocity in the lower prechamber part, but does not significantly affect the global flow pattern (Fig. 13(a)). The higher axial velocity originates in larger nozzle outlet recirculation zones, which consequently reduce the effective flow cross section. The suppression of the recirculation zone in the prechamber bottom reduces strongly the local dissipation of turbulence and therefore results in a more efficient transfer in the upper part (Fig. 12). The creation of a dome in the prechamber bottom (β) has little influence on the flow velocity in the vicinity of the ignition point (Fig. 13(a)), but increases significantly the level of turbulence in this region (Fig. 13(b)). The higher flow velocity in the lower prechamber part accelerates the transfer of unburnt mixture to the upper part, which results in a faster rise in fuel to air equivalence ratio at the ignition point (Fig. 13(c)). The creation of a protuberance to even better lead the incoming

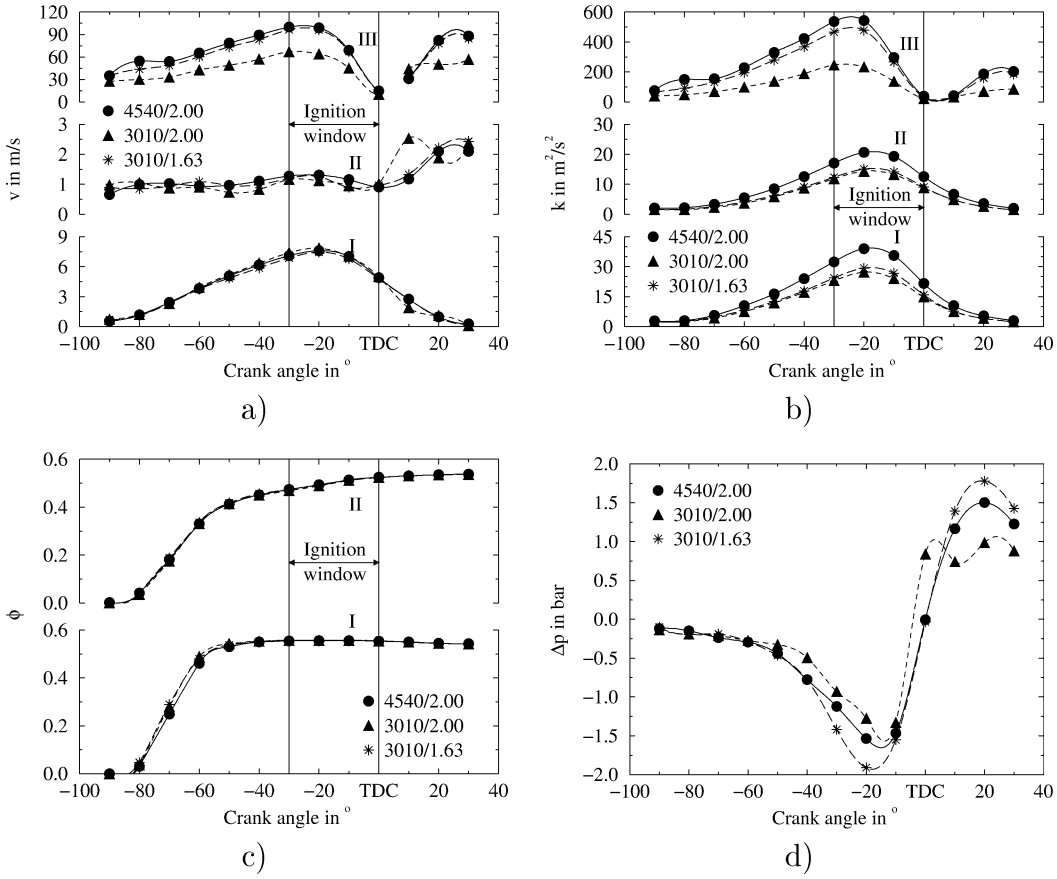

Fig. 11. Influence of the prechamber volume on the flow at different locations in the prechamber ($N_n = 6$, $\alpha_n = 60°$): (a) velocity magnitude, (b) turbulence kinetic energy, (c) fuel to air equivalence ratio, (d) pressure difference between pre- and main chamber.

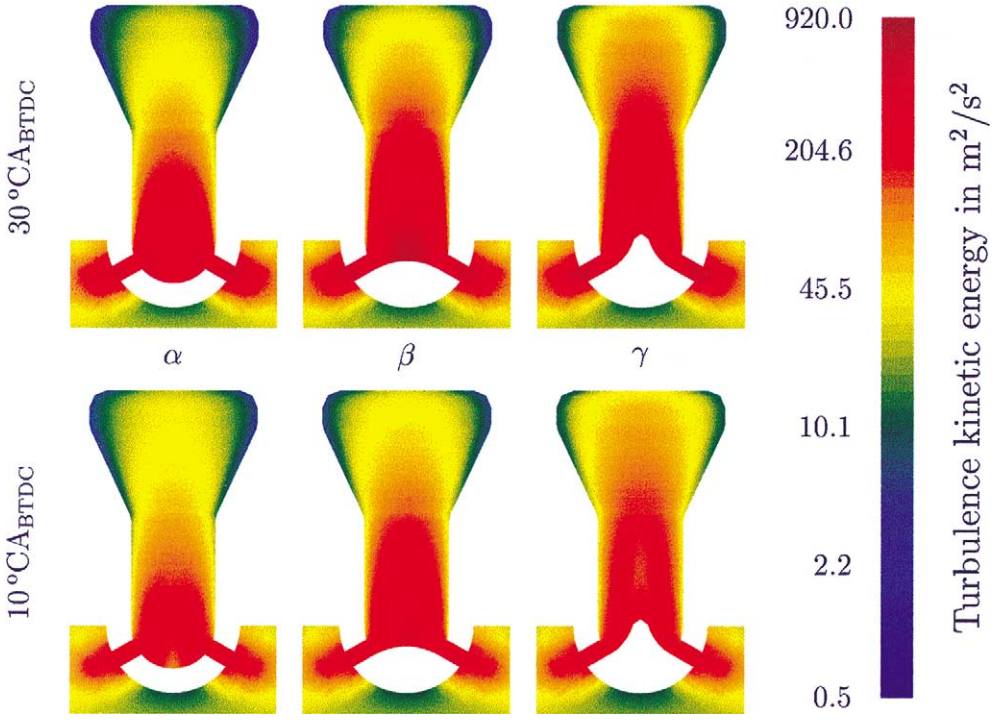

Fig. 12. Influence of the prechamber bottom geometry on the distribution of turbulence kinetic energy ($V_p = 4540$ mm^3, $d_n = 2$ mm, $N_n = 6$, $A_n = 18.85$ mm^2, $\alpha_n = 60°$).

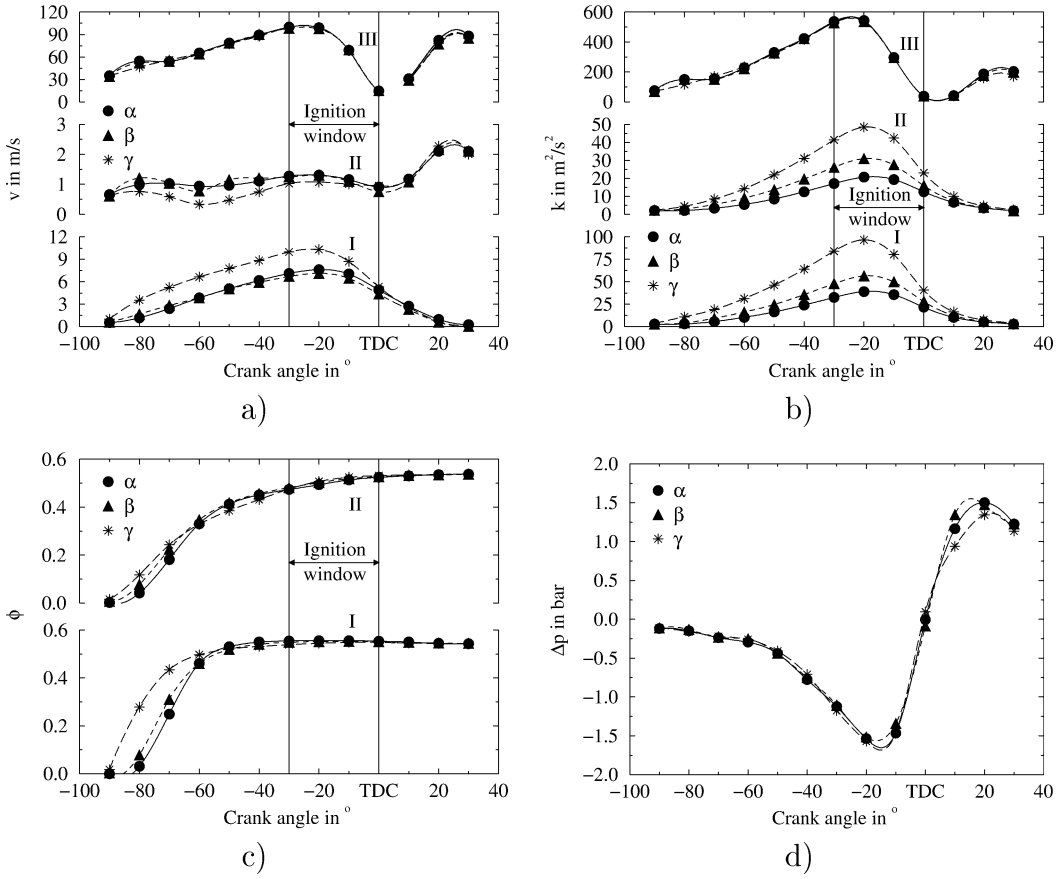

Fig. 13. Influence of the prechamber bottom geometry on the flow at different locations in the prechamber ($V_p = 4540$ mm^3, $d_n = 2$ mm, $N_n = 6$, $A_n = 18.85$ mm^2, $\alpha_n = 60°$): (a) velocity magnitude, (b) turbulence kinetic energy, (c) fuel to air equivalence ratio, (d) pressure difference between pre- and main chamber.

flow (γ) increases further the velocity and turbulence kinetic energy at the ignition location. The much higher axial velocity in the lower part contributes to an even more rapid transfer of unburnt mixture in this region. In both cases, the higher turbulence intensity in the upper part accelerates the incorporation of the residual gas into the unburnt mixture, which reduces somewhat the maximum fuel to air equivalence ratio in the ignition window. Finally, the change in prechamber bottom geometry has no perceptible effect on the pressure drop across the nozzle orifices during compression (Fig. 13(d)), which indicates a similar filling.

4.9. Prechamber internal shape

An insight into the influence of the prechamber internal shape on the flow characteristics was established on the basis of three distinct cases (Fig. 14). In order to allow a significant geometrical variation in the available space of the cylinder head, a reduced prechamber volume of 3000 mm^3 was considered. The first case (α) corresponds to a uniform radial reduction of the base prechamber. The proportion of volume located in the upper part was then reduced (β) and increased (γ), respectively. With a value of 19.64 mm^2, the cross-sectional area of the lower prechamber part of case γ approaches the total area of the nozzle orifices. Therefore, this part acts almost like a prolongation of the orifices up to the main prechamber volume. The mesh used was adapted to each case, but the total number of cells remained the same as for the base case (8714).

The geometry variation has only a very weak effect on the nozzle flow (Fig. 15(a)) and the corresponding turbulence generation (Fig. 15(b)). However, the volume distribution between lower and upper prechamber parts governs the internal flow pattern and thereby the velocity distribution and intensity that determine the transfer of turbulence (Fig. 14) and unburnt mixture towards the ignition point. On the one hand, an increase of the lower part volume in order to achieve a more uniform distribution along the axis (β) reduces to a large extent the velocity magnitude and the turbulence kinetic energy at the ignition point. This consequently delays the arrival of unburnt mixture, and thus leads to a slightly lower fuel to air equivalence ratio at the beginning of the ignition window (Fig. 15(c)). On the other hand, a reduction of the lower part volume in order to form a more compact cavity (γ) generates very high velocity and turbulence kinetic energy in the vicinity of the ignition location, which creates flammable conditions much more rapidly. However, the velocity and turbulence intensity

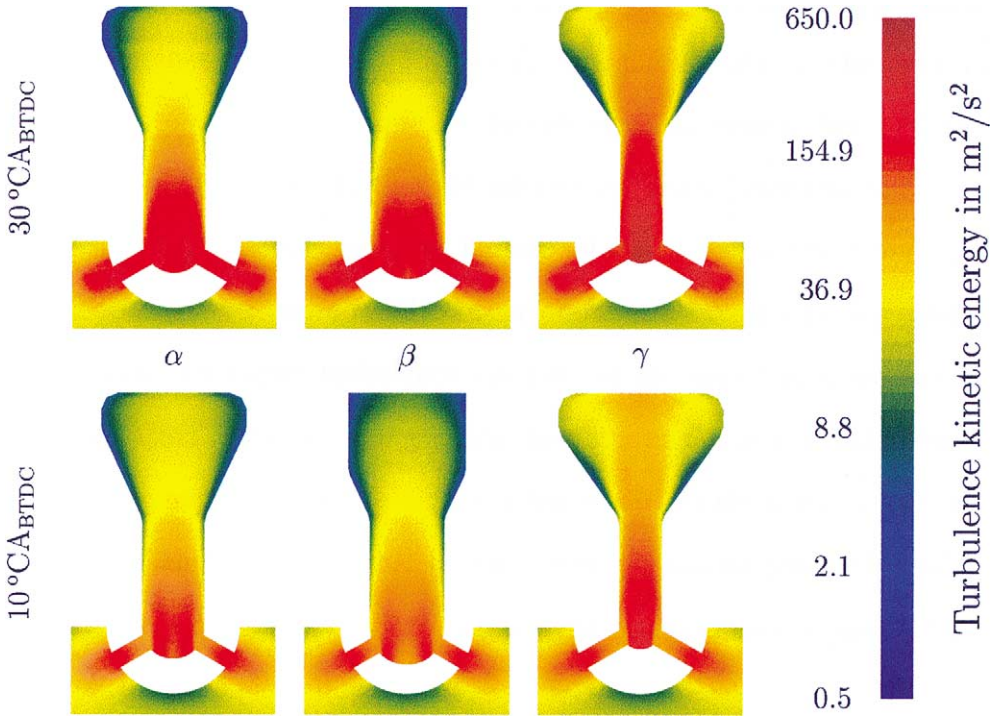

Fig. 14. Influence of the prechamber shape on the distribution of turbulence kinetic energy ($V_p = 3000$ mm^3, $d_n = 2$ mm, $N_n = 6$, $A_n = 18.85$ mm^2, $\alpha_n = 60°$).

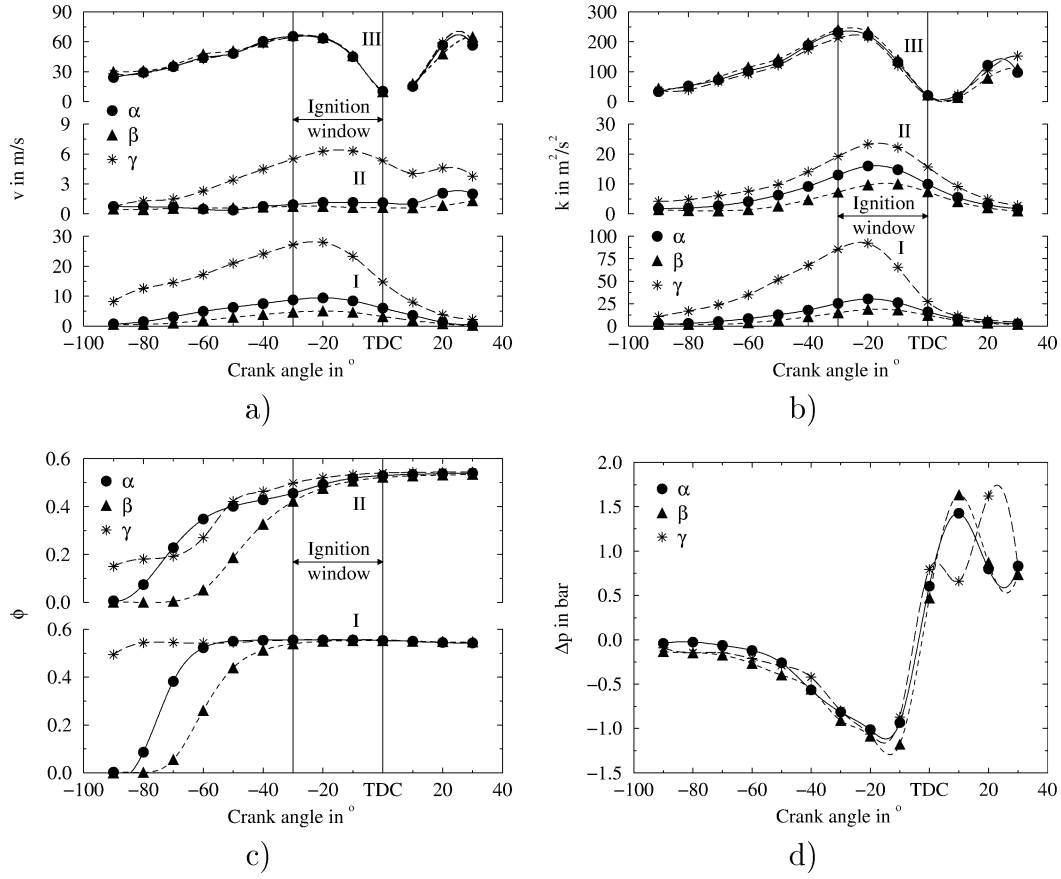

Fig. 15. Influence of a prechamber shape on the flow at different locations in the prechamber ($V_p = 3000$ mm^3, $d_n = 2$ mm, $N_n = 6$, $A_n = 18.85$ mm^2, $\alpha_n = 60°$): (a) velocity magnitude, (b) turbulence kinetic energy, (c) fuel to air equivalence ratio, (d) pressure difference between pre- and main chamber.

reached in this case are much higher than those characterising the conventional combustion chamber (Fig. 5). These conditions could excessively perturb the ignition process and therefore not be practical. An almost equal pressure drop across the nozzle orifices for all the three cases (Fig. 15(d)) indicates a similar prechamber charge.

5. Conclusions

The prechamber numerical study shows that the velocity magnitude at the ignition point is mainly dependent on the prechamber shape, and that it is generally of the same order as with direct ignition. The turbulence intensity varies strongly with the geometrical configuration and reaches, in most cases, a much higher value in the prechamber than in the conventional combustion chamber. High turbulence intensity promotes rapid prechamber combustion, but also perturbs the ignition process and the early stage of the flame kernel growth, which is expected to increase the probability of ignition failure. The partial dilution of the unburnt mixture with unscavenged prechamber residual gas generally leads to a slightly lower fuel to air equivalence ratio than in the case of direct ignition. However, nozzle orifices imparting a swirl motion or a prechamber shape with an almost uniform cross section can result in fuel concentration very close to or beyond the flammability limit. In most cases, the mixture temperature is not significantly affected by changes in the prechamber geometrical configuration. However, depending on the prechamber spark timing, the mixture temperature prevailing at ignition can be similar to or much higher ($\approx$100 K) than in the conventional combustion chamber. The prechamber charge, and thereby the amount of energy available for the main chamber ignition, depends mainly on the prechamber volume, but is significantly affected by the pressure drop across the nozzle orifices.

Acknowledgements

This research work was carried out at the *Laboratory for Industrial Energy Systems (LENI)* of the *Swiss Federal Institute of Technology of Lausanne (EPFL)*. It was financially supported by the *Swiss Federal Office of Energy (OFEN)*, under the grant no 69 801, the engine manufacturer *Liebherr Machines Bulle S.A.*, the cogeneration group manufacturer *Dimag S.A.*, the *Research Fund of the Gas Industry (FOGA)*, as well as by the *EPFL*, who are all gratefully acknowledged.

References

[1] Le Conseil fédéral suisse, Ordonnance sur la protection de l'air (OPair) du 16 décembre 1985 (Etat au 12 octobre 1999).

[2] R.-P. Roethlisberger, G. Leyland, C.-A. Paschoud, D. Favrat, Swiss Motor, Modification d'un moteur Diesel pour le fonctionnement avec mélange stœchiométrique ($\lambda = 1$) et pauvre ($\lambda \gg 1$), Swiss Federal Office of Energy, Final Report, 1998.

[3] R.-P. Roethlisberger, G. Leyland, D. Favrat, R.-R. Raine, Study of a small size cogeneration gas engine in stoichiometric and lean burn modes: Experimentation and simulation, SAE Paper 982451 and SP-1391, 1998.

[4] R.-P. Roethlisberger, D. Favrat, Investigation of the prechamber geometrical configuration of a natural gas spark ignition engine for cogeneration: Part II. Experimentation, Internat. J. Therm. Sci. 42 (3) (2003), to appear.

[5] J.-B. Heywood, Internal Combustion Engine Fundamentals, in: Automotive Technology Series, McGraw-Hill, New York, 1988.

[6] R.-P. Roethlisberger, An experimental investigation of a lean burn natural gas prechamber spark ignition engine for cogeneration, Swiss Federal Institute of Technology of Lausanne, Thesis n^{o} 2346, 2001, also published under Swiss Motor, Modification d'un moteur diesel pour le fonctionnement au gaz naturel en cogeneration, fonctionnement avec préchambre de combustion, Swiss Federal Office of Energy, Final Report, 2001 (in English).

[7] A.-A. Amsden, KIVA-3V: A block-structured KIVA program for engines with vertical and canted valves, Los Alamos National Laboratory report LA-13313-MS, 1997.

[8] N. Nordin, KIVA to EnSight Interface, Department of Thermo and Fluid Dynamics, Chalmers University of Technology, Gothenburg, Sweden, www.tfd.chalmers.se/~nordin/ensight.html, 1998.

[9] A.-A. Amsden, KIVA-3: A KIVA program with block-structured mesh for complex geometries, Los Alamos National Laboratory report LA-12503-MS, 1993.

[10] A.-A. Amsden, P.-J. O'Rourke, T.-D. Butler, KIVA-II: A computer program for chemically reactive flows with sprays, Los Alamos National Laboratory report LA-11560-MS, 1989.

[11] N. Chigier, Energy, Combustion and Environment, in: Energy, Combustion and Environment Series, McGraw-Hill, New York, 1981, ISBN 0-07-010766-1.

[12] I. S̃auperl, S. Laiminger, T. Sams, G. Herdin, D. Plohberger, CFD unterstützte Optimierung eines Großgasmotors, in: Institute for Internal Combustion Engines and Thermodynamics, Graz University of Technology, Austria, 6th Symposium on the Working Process of the Internal Combustion Engine, 1997, pp. 141–155.

[13] T. Nakazono, Characteristics of unburned HC from a Lean–Burn prechamber gas engine, Trans. Japan Soc. Mech. Engrg. (JSME), Ser. B 60 (569) (1994) 335–340 (in Japanese).

[14] E.-O. Reinbold, The AT27GL: A continuing development of the waukesha AT series gas engine, in: Heavy Duty Engines: A Look at the Future, in: ICE, Vol. 22, ASME, 1994, pp. 23–30.

[15] T. Nakazono, Study of lean burn gas engine (effect of main chamber), Trans. JSME, JSME Internat. J. Ser. B 37 (3) (1994) 677–682.

[16] W.-E. Snyder, S.-G. Dexter, Looking into a lean burn spark ignited gas engine, in: The Thirteenth Annual Energy-Sources Technology Conference and Exhibition, New Orleans, Luisiana, January 14–18, 1990, pp. 67–75.

[17] T. Sakurai, F. Shoji, Study on mixture formation in prechamber of lean burn gas engine, in: Spring Technical Conference, in: ICE, Vol. 26-1, ASME, 1996, pp. 43–51.

[18] J. Czerwinski, Über die Zündung und Verbrennung im 4-Takt-Ottomotor mit unterteiltem Brennraum, in: Fortschritt-Berichte des Vereins Deutscher Ingenieure (VDI), Reihe 6: Energitechnik/Wärmetechnik, Vol. 176, 1985.